Physical-layer Network Coding in Two-Way Heterogeneous Cellular Networks with Power Imbalance

Ajay Thampi, *Student Member, IEEE,* Soung Chang Liew, *Fellow, IEEE,* Simon Armour, Zhong Fan, Lizhao You, *Student Member, IEEE,* Dritan Kaleshi

Abstract

The growing demand for high-speed data, quality of service (QoS) assurance and energy efficiency has triggered the evolution of 4G LTE-A networks to 5G and beyond. Interference is still a major performance bottleneck. This paper studies the application of physical-layer network coding (PNC), a technique that exploits interference, in heterogeneous cellular networks. In particular, we propose a rate-maximising relay selection algorithm for a single cell with multiple relays assuming the decode-and-forward strategy. With nodes transmitting at different powers, the proposed algorithm adapts the resource allocation according to the differing link rates and we prove theoretically that the optimisation problem is log-concave. The proposed technique is shown to perform significantly better than the widely studied selection-cooperation technique. We then undertake an experimental study – on a software radio platform – of the decoding performance of PNC with unbalanced SNRs in the multiple-access transmissions. This problem is inherent in cellular networks and it is shown that with channel coding and decoders based on multiuser detection and successive interference cancellation, the performance is better with power imbalance. This paper paves the way for further research in multi-cell PNC, resource allocation, and the implementation of PNC with higher-order modulations and advanced coding techniques.

Index Terms

Physical-layer Network Coding, PNC, Interference, Cooperation, Cellular Networks, LTE-A, WiMAX, CoMP, Heterogeneous Networks, HetNet, Relay Selection, Software Radio, USRP

I. Introduction

As operators evolve their networks toward the 4th generation (4G) Long Term Evolution-Advanced (LTE-A), the research community has moved on to the study of technologies to be adopted in the 5th generation (5G). The evolution to 5G is triggered by the forecast explosion in mobile data traffic, which is expected to grow 7-fold from 2013 to 2017 [1]; 66% of that mobile traffic is expected to be video by 2017 with an increasing number of devices requiring high-speed wireless broadband.

In LTE-A systems, attempts to address these requirements are made by cell size reduction and aggressive frequency reuse. As a result, interference between cell sites is identified as the major performance bottleneck [2], [3] and techniques such as coordinated multipoint (CoMP) transmission and reception and heterogeneous networks (HetNet) have been proposed [4]. In a CoMP-based HetNet, the base station and users coordinate their transmissions and receptions with the help of many low-powered nodes such as relays, femtocells, picocells and remote radio heads. Such systems are shown to have improved cell coverage and also spectral efficiency [5], [6]. In this paper, we consider a HetNet where there are multiple relays in the cell to assist with transmission and reception. These relays aid in coverage extension by improving the performance for users at the cell edge. In a CoMP-based HetNet, further performance gains can be achieved by employing physical-layer network coding (PNC).

PNC was first proposed in 2006 [7], [8] as a way to exploit interference inherent in wireless communication systems. Rather than treating interference as a source of signal corruption, PNC exploits the natural network coding operation that occurs when the desired and interfering electromagnetic waves superimpose with each other. Compared with the traditional non-network-coded scheme (TS), PNC could achieve a 100% throughput gain [9]. Since its inception, PNC has gained a wide following in the research community and has recently been considered as a study item in the 3GPP standards [10]–[12].

A. Related Work

To date, most PNC studies have focused on the two-way relay channel (TWRC) model where all the nodes transmit at equal powers [9]. Two key issues in PNC, symbol asynchrony and channel coding, were addressed in the time domain in [13] and in the frequency domain in [14]. PNC was also successfully implemented on a software radio platform and insights on throughput gains, symbol misalignment, channel coding, effect of carrier frequency offset and real-time issues were gained through these practical prototyping efforts [14]–[16]. In [17],

the spectral efficiency of MIMO systems is further improved by combining it with PNC. One way of combining MIMO and PNC is by precoding at the transmitter to convert the MIMO streams to parallel single-input single-output (SISO) streams. This approach however requires channel knowledge at the transmitter and also strict time and carrier phase synchronisation [17]. The application of PNC in a cellular system where the base station and the relay are equipped with multiple antennas was studied in [18]. In such a system, multiple users could share the same relay with careful precoding at the base station and relay.

In cellular networks, where there are multiple relays deployed in the cell, an important problem is to select the optimum relay to assist the end-to-end information exchange between the base station and the user. In [19] and [20], relay selection was studied in a PNC system where the amplify-and-forward[1] (AF) strategy was adopted at the relays. Both relay selection algorithms were based on minimising the overall sum bit-error-rate, and the optimisation problem was simplified by assuming equal time allocation for all the links. An AF-based PNC system is however known to be limited by noise, especially at low signal-to-noise ratios (SNRs) [21]. For instance, when the SNR is between 5-7.5 dB in a symmetric TWRC, the achievable rate of ANC reduces by 5-22% when compared to TS [9]. The performance limitation due to noise could be mitigated by adopting the decode-and-forward[2] (DF) strategy at the relays [9]. At low SNRs (5-7.5 dB) in a symmetric TWRC, DF-based PNC still performs better than TS, achieving a rate gain of 20-27%. The DF strategy is therefore considered in this paper.

Relay selection in a DF-based PNC system was studied in [22]. The algorithm, called SC-PNC, is based on the widely applied selection-cooperation technique [23], [24] and consists of two steps. In the first step, the end nodes transmit their symbols in the multiple-access phase and all the relays that are not in outage are added to a list for selection. In the second step, the relay in the list that minimises the broadcast-phase outage probability or maximises the minimum mutual information of the two broadcast links is selected. This algorithm assumes equal time allocation for all the links and a closed-form expression for the outage probability is derived.

The drawback of the approach in [22] is that the relay selected to maximise the minimum

[1]The relay amplifies the received superimposed network coded symbol and forwards it to the end nodes.

[2]The relay decodes the superimposed network coded symbol rather than the individual symbols transmitted by the end nodes.

mutual information of the two broadcast links may not be the optimum one for the multiple-access phase. This suboptimal selection could affect the overall rate of the PNC system. We have also seen that the relay selection algorithms in the literature are simplified by assuming equal time allocation for all the links. The performance of the system could be further improved by allocating more time for the weaker link. In addition, the problem of power imbalance, which is inherent in a cellular network, has not been studied. Since all the nodes transmit at different powers, the decoding performance at the relay in the multiple-access phase could be impacted. All the above gaps are addressed in this paper.

B. Contributions

We consider a PNC system where the nodes transmit at different powers and the time slots allocated for the links are made inversely proportional to their achievable rates. Our objective is to maximise the overall rate of the PNC system and with imbalanced transmitted powers, this necessitates allocating more time for the node with the weaker link. To the best of our knowledge, such a system has not been studied in the literature and we call it PNC-B. We prove that the optimisation problem is log-concave and propose a gradient-ascent based algorithm for relay selection. The performance of PNC-B, in terms of overall rate and densification gain, is shown to be much better than SC-PNC [22].

We then study the decoding performance of the relay in the multiple-access phase, given the power imbalance in the system. An experimental study on a software radio platform is conducted. We show that with link-by-link channel coding, the decoding success rate is better when there is an imbalance in power. In addition, we show that power control to balance the SNRs could be detrimental to the performance, especially at low SNRs.

The rest of the paper is structured as follows. Section II gives an overview of the system model adopted in this paper. Section III then studies the transmission strategies and their corresponding information-theoretic rates. In Section IV, we look at the relay selection problem for PNC-B. The proof that the optimisation problem is log-concave and the derivation of the algorithm can be found in Section IV-A. The simulations results comparing the performance of the proposed PNC-B algorithm with SC-PNC [22] can be found in Section IV-B. Section V describes the software radio experimental setup and analyses the decoding performance of PNC-B for various SNRs. Finally, Section VI concludes the paper and suggests avenues for further research.

II. System Model

The system consists of a cell served by a single base station with multiple users and relays. The traffic between the base station and the users is bidirectional. We assume that the relays are equipped with a single antenna and hence, every scheduled user will have a unique relay assisting it. Both the linear and planar network models are considered, as shown in Figures 1a and 1b respectively.

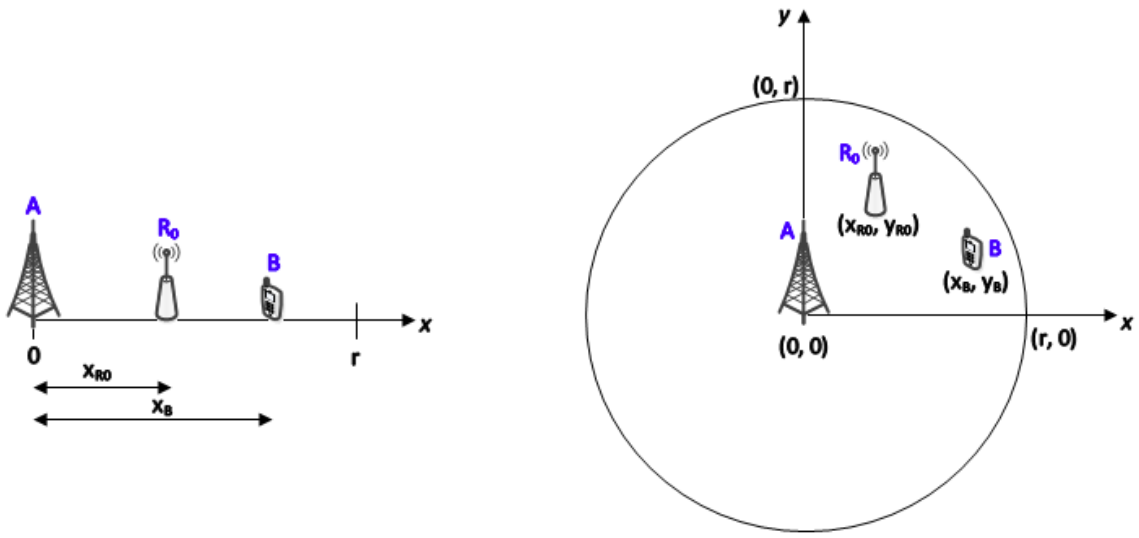

(a) Linear Model

(b) Planar Model

Fig. 1: Network Models

The figures show a single scheduled user and a unique relay assisting it. In both models, the base station is represented as node A, the user as node B and the optimum relay assisting them as node R_0. Each node is equipped with a single omnidirectional antenna. The cell radius is denoted by r and the base station is placed at the origin in both models. In the linear model, the relay and user are at distances x_{R_0} and x_B respectively from the base station. In the planar model, the locations of the relay and user are Cartesian coordinates, (x_{R_0}, y_{R_0}) and (x_B, y_B) respectively. For the relay selection problem, we first consider the linear model to keep the equations simple and then extend the derived algorithm to the planar model. We also first analyse the performance results of the selection algorithm for the single-user case and then describe the scheduling algorithm for the multi-user case.

In general, the received power at node y when node x transmits at power $P_x^{(t)}$ is given by

$$P_{xy}^{(r)} = \bar{P}_x |h_{xy}|^2 d_{xy}^{-n} \tag{1}$$

where n is the path loss exponent, and $|h_{xy}|$ and d_{xy} are the normalised gain of the channel and the distance between nodes x and y, respectively. The path loss exponent is assumed to be the same for all the links since it is assumed that the base station, relay and users are deployed in the same environment (typically dense-urban or urban). In (1), $\bar{P}_x$ is the received power from node x accounting for the free space path loss, given by

$$\bar{P}_x = \left(\frac{c}{4\pi f_c}\right)^2 d_0^{n-2} P_x^{(t)} \tag{2}$$

where c is the speed of light in vacuum, f_c is the carrier frequency, d_0 is the reference distance and $P_x^{(t)}$ is the transmitted power of node x.

In cellular networks, it is fair to assume the following constraint on the transmitted powers.

$$P_A^{(t)} > P_{R_0}^{(t)} > P_B^{(t)} \tag{3}$$

This form of power imbalance is considered in this paper. Without loss of generality, time-division duplexing is assumed and all nodes in the network respect the half-duplex constraint since full-duplex wireless is presently very challenging to implement.

III. Transmission Strategies and Rates

The PNC scheme is shown in Figure 2. In the first time slot, called the multiple-access phase, the base station and user (nodes A and B respectively) transmit simultaneously. The relay tries to deduce a network coded message from the superimposed signals of A and B in the multiple-access phase. This process is called PNC mapping and is described in great detail in [9]. In the second time slot, called the broadcast phase, the relay broadcasts the deduced network-coded message (stored at the relay) to the base station and the user. Using its self-information, each end node can extract the signal transmitted by the other.

The rate of the multiple-access phase is upper-bounded by (4) below. If link-by-link channel coding is done in the PNC system, where the relay performs channel decoding and re-encoding in addition to PNC mapping [9], then it is shown in [25] that the upper bound can be approached within 1/2 bit using nested lattice codes. The rate of the multiple-access phase using lattice codes is given by (5) below. For mathematical tractability, we will use the upper-bound rate equation (4) for the theoretical derivations in the next section. We will however use (5) to validate that the relay selection algorithm derived using the upper-bound approximation is optimum for a practical system using nested lattice codes.

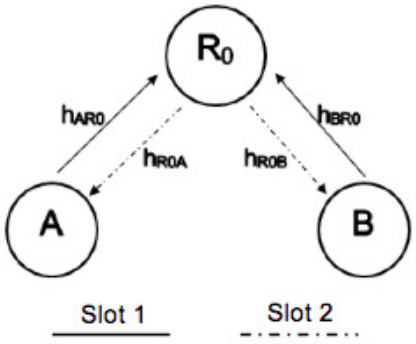

Fig. 2: Physical-Layer Network Coding

$$R_{MA} = \min\left\{\log_2\left(1+\frac{P_{AR_0}^{(r)}}{N_0 W}\right), \log_2\left(1+\frac{P_{BR_0}^{(r)}}{N_0 W}\right)\right\} \text{ bps/Hz} \tag{4}$$

$$R_{MA}^{LC} = \min\left\{\log_2\left(\frac{P_{AR_0}^{(r)}}{P_{AR_0}^{(r)}+P_{BR_0}^{(r)}}+\frac{P_{AR_0}^{(r)}}{N_0 W}\right), \log_2\left(\frac{P_{BR_0}^{(r)}}{P_{AR_0}^{(r)}+P_{BR_0}^{(r)}}+\frac{P_{BR_0}^{(r)}}{N_0 W}\right)\right\} \text{ bps/Hz} \tag{5}$$

For the broadcast phase, the rate is given by (6).

$$R_{BC} = \min\left\{\log_2\left(1+\frac{P_{R_0A}^{(r)}}{N_0 W}\right), \log_2\left(1+\frac{P_{R_0B}^{(r)}}{N_0 W}\right)\right\} \text{ bps/Hz} \tag{6}$$

The overall achievable rate of the PNC system with equal time-slot allocation, as assumed in the literature [19], [20], [22], is given by (7).

$$R_{PNC} = \frac{1}{2}\min\left\{R_{MA}^{LC}, R_{BC}\right\} \text{ bps/Hz} \tag{7}$$

For the PNC system considered in this paper with rate-maximizing unbalanced time allocation, the overall achievable rate is given by (8).

$$R_{PNC-B} = \min\left\{\rho_{MA} R_{MA}^{LC}, \rho_{BC} R_{BC}\right\} \text{ bps/Hz} \tag{8}$$

where ρ_{MA} and ρ_{BC} are the fractions of time allocated for the multiple-access and broadcast phases respectively. In order to maximise the rate, the time allocated for each phase has to

be inversely proportional to their achievable rate, i.e. more time has to be allocated for the weaker link. This is given by (9) and (10) respectively.

$$\rho_{MA} = \frac{R_{BC}}{R_{MA}^{LC} + R_{BC}} \tag{9}$$

$$\rho_{BC} = \frac{R_{MA}}{R_{MA}^{LC} + R_{BC}} \tag{10}$$

Using (9) and (10), (8) reduces to,

$$R_{PNC-B} = \frac{R_{MA}^{LC} R_{BC}}{R_{MA}^{LC} + R_{BC}} \text{bps/Hz} \tag{11}$$

IV. Relay Selection for PNC-B

A. The Algorithm

This sub-section addresses the problem of relay selection for the PNC-B transmission strategy. We first restrict our study, as in [22], to the single user case and will later describe the scheduling algorithm for the multi-user case. To the best of our knowledge, this has not been studied in the literature. The SC-PNC approach in [22] cannot be easily extended to PNC-B as the derivation of the outage probability becomes mathematically intractable.

The optimum relay is the one that maximises the overall rate of the PNC-B system given by (12).

$$\tilde{R}_{PNC-B} = \frac{R_{MA} R_{BC}}{R_{MA} + R_{BC}} \text{bps/Hz} \tag{12}$$

In (12), the upper bound rate for the multiple-access phase, given by (4), is used for analytical simplicity. If the rate using nested lattice codes, given by (11) is used, the optimisation problem becomes mathematically intractable. It will however be shown in Section IV-B that the optimum relay derived using the upper-bound approximation in turn maximises the achievable rate using nested lattice codes.

R_{MA} and R_{BC}, given by (4) and (6) respectively, can be rewritten as $R_{MA} = \min\{R_{AR_0}, R_{BR_0}\}$ and $R_{BC} = \min\{R_{R_0A}, R_{R_0B}\}$. In order to keep the equations simple, we first consider the linear model as shown in Figure 1a. The derived relay selection algorithm will then be extended to the planar model shown in Figure 1b for the single-user case.

Lemma 1. *The overall rate of the PNC-B system, dependent on the user and relay locations,*

consists of four cases given by,

$$\tilde{R}_{PNC-B} = \begin{cases} \frac{R_{AR_0}R_{R_0A}}{R_{AR_0}+R_{R_0A}} & \textit{if } x_{R_0} \in \left(\frac{x_B}{D}, x_B\right] \\ \frac{R_{AR_0}R_{R_0B}}{R_{AR_0}+R_{R_0B}} & \textit{if } x_{R_0} \in \left(\frac{x_B}{D}, \frac{x_B}{2}\right] \\ \frac{R_{BR_0}R_{R_0A}}{R_{BR_0}+R_{R_0A}} & \textit{if } x_{R_0} \in \left(\frac{x_B}{2}, \frac{x_B}{D}\right] \\ \frac{R_{BR_0}R_{R_0B}}{R_{BR_0}+R_{R_0B}} & \textit{if } x_{R_0} \in \left[d_0, \frac{x_B}{2}\right] \end{cases} \tag{13}$$

where $D = 1 + \left(P_B^{(t)}/P_A^{(t)}\right)^{1/n}$.

Proof: From (4), $R_{MA} = R_{AR_0}$ when $R_{AR_0} < R_{BR_0}$ and $R_{MA} = R_{BR_0}$ otherwise. When $R_{AR_0} < R_{BR_0}$,

$$\begin{aligned} &\log_2\left(1 + \frac{P_{AR_0}^{(r)}}{N_0 W}\right) < \log_2\left(1 + \frac{P_{R_0B}^{(r)}}{N_0 W}\right) \\ &\log_2\left(1 + \frac{\bar{P}_A |h_{AR_0}|^2 x_{R_0}^{-n}}{N_0 W}\right) < \\ &\log_2\left(1 + \frac{\bar{P}_B |h_{BR_0}|^2 \left|x_B - x_{R_0}\right|^{-n}}{N_0 W}\right) \end{aligned} \tag{14}$$

Ignoring the effects of fading and considering that the optimum relay has to lie between the base station and the user, (14) reduces to

$$P_A^{(t)} x_{R_0}^{-n} < P_B^{(t)} (x_B - x_{R_0})^{-n} \tag{15}$$

Solving (15) for x_{R_0}, we can obtain the range of values for which $R_{MA} = R_{AR_0}$ which are, $x_{R_0} \in \left(\frac{x_B}{D}, x_B\right)$ where $D = 1 + \left(P_B^{(t)}/P_A^{(t)}\right)^{1/n}$. On the other hand, $R_{MA} = R_{BR_0}$ when $x_{R_0} \in \left[d_0, \frac{x_B}{D}\right]$.

Similarly, from (6), $R_{BC} = R_{R_0A}$ when $R_{R_0A} < R_{R_0B}$ and $R_{BC} = R_{R_0B}$ otherwise. Thus from $R_{R_0A} < R_{R_0B}$, we get

$$P_{R_0}^{(t)} x_{R_0}^{-n} < P_{R_0}^{(t)} (x_B - x_{R_0})^{-n} \tag{16}$$

Equation (16) is obtained similar to (15). Solving (16) for x_{R_0}, we get $R_{BC} = R_{R_0A}$ when $x_{R_0} \in \left(\frac{x_B}{2}, x_B\right)$ and $R_{BC} = R_{R_0B}$ when $x_{R_0} \in \left[d_0, \frac{x_B}{2}\right]$. Combining these results for R_{MA} and R_{BC}, we can obtain (13). ■

The purpose of Lemma 1 is to show the four different search spaces for the optimum relay and the corresponding rate equations. By ignoring the effects of fading in Lemma 1, we are assuming that the choice of the optimum relay is mostly determined by path loss and the average received power. Although it is not accurate, this assumption allows for a simpler formulation of the search space as will be seen in Lemma 2. Since the search space is wide

enough, any deviation in the optimum relay location due to fading will still be within the search space. We will show this by reintroducing fading in the simulation-based study in Section IV-B.

Furthermore, the effects of fading are ignored to decouple the problem of relay selection from resource allocation. In an OFDM system, the effects of wideband (frequency-selective) fading are mitigated by dividing the signal into many narrowband subcarriers. Maximising performance in such a flat fading environment is then a resource allocation issue. In [26], the problem of subcarrier allocation in an OFDMA-based heterogeneous system that employed straightforward network coding was studied. For a PNC system, this problem would alter slightly since the same subcarriers would need to be used by the base station and the user in the multiple-access phase. This is however beyond the scope of this paper and will be addressed in the future.

Lemma 2. *The search for the optimum relay can be restricted to the range* $\left(\frac{x_B}{2}, \frac{x_B}{D}\right]$.

Proof: To prove this lemma, the validity of the four cases in Lemma 1 have to be analysed. Given the power constraint (3) where $P_A^{(t)} > P_B^{(t)}$, the constant D is less than 2. Hence, $\frac{x_B}{D} > \frac{x_B}{2}$ which makes Case 2, where $x_{R_0} \in \left(\frac{x_B}{D}, \frac{x_B}{2}\right]$, invalid. For Case 1 where $x_{R_0} \in \left(\frac{x_B}{D}, x_B\right]$, the optimisation problem will be skewed towards the user since a relay closer to the user will be chosen. Similarly, Case 4 will be skewed towards the base station since a relay in the range $\left[d_0, \frac{x_B}{2}\right]$ will be chosen. Thus, the search space for the optimum relay must be the one in Case 3 where $x_{R_0} \in \left(\frac{x_B}{2}, \frac{x_B}{D}\right]$. ■

Using Lemmas 1 and 2, (12) simplifies to (17) below.

$$\tilde{R}_{PNC-B} = \frac{R_{BR_0} R_{R_0A}}{R_{BR_0} + R_{R_0A}} \; ; \; x_{R_0} \in \left(\frac{x_B}{2}, \frac{x_B}{D}\right] \tag{17}$$

The objective function for PNC-B is then

$$f(x_{R_0}) = \left(\frac{1}{\log_e 2}\right) . \frac{g(x_{R_0}) h(x_{R_0})}{g(x_{R_0}) + h(x_{R_0})} \tag{18}$$

In (18),

$$g(x_{R_0}) = \log_e \left(1 + \Gamma_B (x_B - x_{R_0})^{-n}\right) \tag{19}$$

$$h(x_{R_0}) = \log_e \left(1 + \Gamma_{R_0} x_{R_0}^{-n}\right) \tag{20}$$

where $\Gamma_B = \frac{\bar{P}_B |h_{BR_0}|^2}{N_0 W}$ and $\Gamma_{R_0} = \frac{\bar{P}_{R_0} |h_{R_0A}|^2}{N_0 W}$. The objective function is basically the rate of the PNC-B system, given by (17), converted to the natural unit of information (nat). The

relay selection problem for the linear model can be formulated as

$$\begin{aligned} \underset{x_{R_0}}{\text{maximise}} \quad & f(x_{R_0}) \\ \text{subject to} \quad & \frac{x_B}{2} < x_{R_0} \leq \frac{x_B}{D} \\ & |x_B - x_{R_0}| \geq d_0 \end{aligned} \tag{21}$$

The following lemmas and theorem will help design the algorithm to solve (21).

Lemma 3. *If a function f on $\mathbb{R}$ is twice differentiable, then it is log-concave if and only if **dom** f is a convex set and $f''(x)f(x) \leq f'(x)^2, \forall x \in$ **dom** f [27].*

Lemma 4. *Log-convexity and log-concavity are closed under multiplication and positive scaling [27].*

Theorem 1. *The objective function for PNC-B is log-concave for $x_{R_0} \in \left(\frac{x_B}{2}, \frac{x_B}{D}\right]$, assuming $\Gamma_B \left(x_B - x_{R_0}\right)^{-n} \gg 1$ and $\Gamma_{R_0} x_{R_0}^{-n} \gg 1$.*

Proof: Taking the logarithm of (18),

$$F = \log_e g + \log_e h - \log_e \left(g + h\right) - \log_e \left(\log_e 2\right) \tag{22}$$

To prove log-concavity, we need to obtain the first and second order derivatives of R_{BR_0} and R_{R_0A}, which are functions $g(x_{R_0})$ and $h(x_{R_0})$ respectively. The first-order derivative of $g(x_{R_0})$ can be obtained to be

$$g'(x_{R_0}) = \frac{n\Gamma_B \left(x_B - x_{R_0}\right)^{-n-1}}{1 + \Gamma_B \left(x_B - x_{R_0}\right)^{-n}} \tag{23}$$

Given the assumption that $\Gamma_B \left(x_B - x_{R_0}\right)^{-n} \gg 1$, (23) becomes (24) since $1 + \Gamma_B \left(x_B - x_{R_0}\right)^{-n} \approx \Gamma_B \left(x_B - x_{R_0}\right)^{-n}$ and the second-order derivative is (25). We discuss the validity of this assumption following the proof.

$$g'(x_{R_0}) \approx \frac{n}{x_B - x_{R_0}} \tag{24}$$

$$g''(x_{R_0}) \approx -\frac{n}{\left(x_B - x_{R_0}\right)^2} \tag{25}$$

Now for $h(x_{R_0})$, the first-order derivative is

$$h'(x_{R_0}) = -\frac{n\Gamma_{R_0} x_{R_0}^{-n-1}}{1 + \Gamma_{R_0} x_{R_0}^{-n}} \tag{26}$$

A similar simplification is made as earlier by assuming that $\Gamma_{R_0} x_{R_0}^{-n} \gg 1$. Equation (26) becomes (27) since $1 + \Gamma_{R_0} x_{R_0}^{-n} \approx \Gamma_{R_0} x_{R_0}^{-n}$ and the second-order derivative is (28).

$$h'(x_{R_0}) \approx -\frac{n}{x_{R_0}} \tag{27}$$

$$h''(x_{R_0}) \approx \frac{n}{x_{R_0}^2} \tag{28}$$

Using (19), (24) and (25), we can obtain

$$g(x_{R_0}) g''(x_{R_0}) \approx -\frac{n \log_e \left(1 + \Gamma_B (x_B - x_{R_0})^{-n}\right)}{\left(x_B - x_{R_0}\right)^2} \tag{29}$$

and

$$g'(x_{R_0})^2 \approx \left(\frac{n}{x_B - x_{R_0}}\right)^2 \tag{30}$$

Since n, Γ_B and $(x_B - x_{R_0})$ are positive, $gg'' < 0$ and $g' > 0$. Thus by Lemma 3, g is log-concave.

Similarly, using (20), (27) and (28), we can obtain

$$h(x_{R_0}) h''(x_{R_0}) \approx \frac{n \log_e \left(1 + \Gamma_{R_0} x_{R_0}^{-n}\right)}{x_{R_0}^2} \tag{31}$$

and

$$h'(x_{R_0})^2 \approx \left(\frac{n}{x_{R_0}}\right)^2 \tag{32}$$

The condition for log-concavity, $hh'' \leq (h')^2$, is satisfied if and only if $x_{R_0} \geq \left(\frac{\Gamma_{R_0}}{e^n - 1}\right)^{\frac{1}{n}}$. For the setup considered in this paper, $\left(\frac{\Gamma_{R_0}}{e^n - 1}\right)^{\frac{1}{n}} < d_0$ and since this is outside the domain of f, h is also log-concave (by Lemma 3).

Now let $j = g + h$. In general, the sum of log-concave functions is not log-concave [27]. So we look at the first and second-order derivates of j given by

$$j'(x_{R_0}) \approx \frac{n \left(2x_{R_0} - x_B\right)}{x_{R_0} \left(x_B - x_{R_0}\right)} \tag{33}$$

and

$$j''(x_{R_0}) \approx -\frac{n x_B \left(2x_{R_0} - x_B\right)}{x_{R_0}^2 \left(x_B - x_{R_0}\right)^2} \tag{34}$$

Since $\mathbf{dom}\ f = \left(\frac{x_B}{2}, \frac{x_B}{D}\right]$, $2x_{R_0} - x_B > 0$. This means that $j' > 0$ and $j'' < 0$. Thus, $jj'' \leq (j')^2$ and hence $j = g + h$ is log-concave (by Lemma 3).

Since g, h and $g + h$ are log-concave, then by Lemma 4, f is also log-concave. ■

In Theorem 1, we assume that $\Gamma_B \left(x_B - x_{R_0}\right)^{-n} \gg 1$ and $\Gamma_{R_0} x_{R_0}^{-n} \gg 1$. This means that the received SNR of user B at the relay R_0 and the received SNR of the relay R_0 at the base

station A are medium or high. For a typical cellular network setup [26] that we consider in this paper, where the user transmits at power 23 dBm and the relay transmits at power 30 dBm, this is a fair assumption provided that relays are deployed in the cell to assist users at the cell edge.

The log-concavity property in Theorem 1 is extremely important for the following reasons:

1) A simple optimisation algorithm such as gradient ascent can be used to find the global optimum relay location, $x^*_{R_0}$.
2) If there is no relay at $x^*_{R_0}$, then the next best option is to choose the one closest to the global optimum solution.
3) The boundary for placing relays for PNC-B is $\frac{r}{D}$, and this will be useful for network planning.

The gradient of $F(x_{R_0})$ can be obtained to be

$$F' = \frac{g'}{g} + \frac{h'}{h} - \frac{g'+h'}{g+h} \tag{35}$$

In order to compute F', Γ_{R_0} and Γ_B have to be obtained which would require channel estimates at the base station and relay respectively. Algorithm 1, which is based on gradient ascent, describes the relay selection process for PNC-B. The parameter α is the step size and the criteria for convergence are:

1) F at iteration $i+1$ is less than that of iteration i, or
2) $x^*_{R_0} > \frac{\hat{x}_B}{D}$

Algorithm 1: Relay Selection (Linear Model)

Estimate the user location $\hat{x}_B$ using received SNR $\frac{P^{(r)}_{AB}}{N_0 W}$;
Initialise $x^*_{R_0} = \frac{\hat{x}_B}{2}$;
repeat
  $x^*_{R_0} := x^*_{R_0} + \alpha F'$ /* F' given by (35) */
until *convergence*;
Return relay closest to $x^*_{R_0}$;

The algorithm requires as input the transmitted powers of each of the nodes and the locations of the deployed relays, which are known a priori. Besides these two inputs, the algorithm also requires the received SNRs from each of the users in the cell in order to estimate its distance from the base station. In the algorithm, the received SNR from the user will be

an estimate based on the reference or training symbol transmitted by the base station. This is typically relayed to the base station through the control channel as measurement reports. In LTE, for instance, the measurement report contains the reference signal received power (RSRP) and the reference signal received quality (RSRQ) [28]. In order to obtain the estimate of the user location ($\hat{x}_B$), the operator could employ the Minimisation of Drive Tests (MDT) reports specified in the 3GPP LTE standards [29]. These reports contain RSRP, RSRQ and detailed location information in the form of GPS coordinates. This information can be used to train a machine learning algorithm that estimates $\hat{x}_B$. This is however beyond the scope of this paper and will be addressed in the future.

The extension of Algorithm 1 to the planar model is straightforward. The optimum relay location will be initialised as $\left(x^*_{R_0}, y^*_{R_0}\right) = \left(\frac{\hat{x}_B}{2}, \frac{\hat{y}_B}{2}\right)$. The objective function f will be dependent on the coordinates (x_{R_0}, y_{R_0}) and the gradients $\frac{\partial F}{\partial x_{R_0}}$ and $\frac{\partial F}{\partial y_{R_0}}$ have to be computed. Note that in each iteration, x_{R_0} and y_{R_0} have to be updated simultaneously. The criteria for convergence is similar to that of the linear model where either,

1) $F\left(x_{R_0}, y_{R_0}\right)$ at iteration $i+1$ is less than that of iteration i, or
2) $\left(x^*_{R_0}, y^*_{R_0}\right) > \left(\frac{\hat{x}_B}{D}, \frac{\hat{y}_B}{D}\right)$

B. Simulation Results

The simulation setup is summarised in Table I. Link-by-link channel coding is done in the PNC system and the achievable rate is computed assuming the use of nested lattice codes [25] in the system. This rate, given by (11), is averaged over 1000 different network realisations.

TABLE I: Simulation Setup

Base Station Transmitted Power, $P_A^{(t)}$	46 dBm
Relay Transmitted Power, $P_{R_0}^{(t)}$	30 dBm
User Transmitted Power, $P_B^{(t)}$	23 dBm
Path Loss Exponent, n	3.7
Cell Radius, r	1 km
Reference Distance, d_0	10 m
Carrier Frequency, f_c	1.9 GHz
Fading Model	Rayleigh
Step Size, α	0.01

Figure 3 shows, as an illustrative example, the achievable rates for different relays for the case of a user located at (850,750) metres, i.e. near the cell edge. This user is represented as a

circle in magenta. Relays, represented as red pluses, are deployed with a separation distance of 200 metres. The achievable rates (in bps/Hz) for the overall system using each relay is shown against the corresponding plus symbol. For instance, if the relay at the top right corner is selected then the PNC system achieves an overall rate of 0.28 bps/Hz. By using Algorithm 1 for the planar model, which is derived using the upper-bound approximation, the relay represented as a blue square is selected for the given user. It can be seen that this relay is optimum as it maximises the overall achievable rate of the system, given by 1.3 bps/Hz.

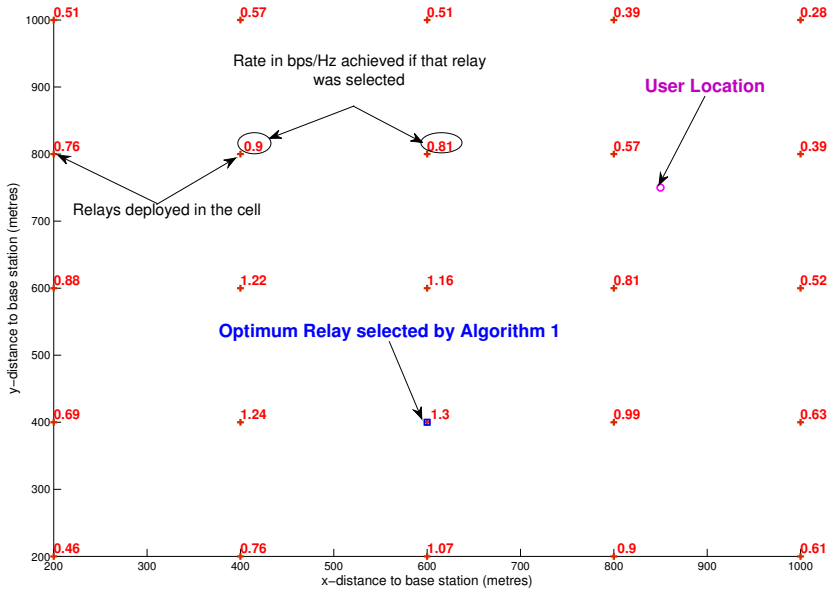

Fig. 3: PNC-B Relay Selection in the Planar Model

With the relay selection algorithm in place, we compare the rates of the proposed PNC-B scheme with that of SC-PNC [22] in Figure 4. Two different network deployments are considered, a dense deployment where relays are placed every 10 metres in the cell (Figure 4a) and a sparse deployment where the relay separation is 400 metres (Figure 4b). It can be seen that PNC-B outperforms SC-PNC for all user locations. In addition, the gain of PNC-B over SC-PNC is more significant for a sparse deployment. Intuitively, this is down to the unequal time-slot allocation in PNC-B. For a dense deployment, the difference in SNRs between the two multiple-access links is smaller than that of a sparse deployment.

Using Lemma 2, the search space for the optimum relay is also reduced drastically. For a user at the cell edge, i.e. at a distance greater than 800 metres from the base station, the search space is reduced by a factor of 11 for the dense deployment and by a factor of 9 in

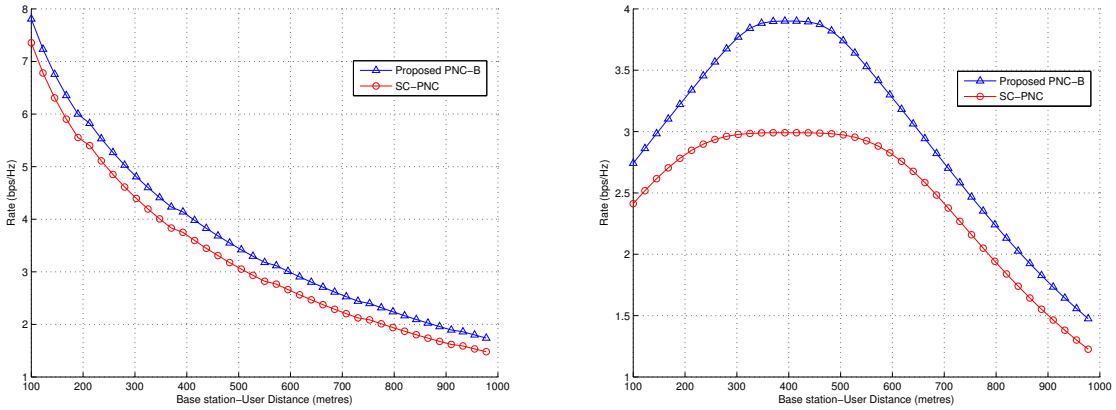

(a) Relay Separation = 10m

(b) Relay Separation = 400m

Fig. 4: Rate Performance Comparison

the sparse deployment.

We now look at another performance metric, called network densification gain, as defined in [30]. The densification gain, ρ in (36), measures the effective increase in the aggregate data rate relative to the increase in base station or relay density. In (36), if the number of relays/km^2 is doubled, then the network density factor = 2.

$$\rho = \frac{\text{Aggregate Rate Gain}}{\text{Network Density Factor}} \tag{36}$$

In Figure 5, the densification gain and rate gain of the proposed PNC-B scheme are compared with that of SC-PNC for various network densities. 100 users were uniformly distributed in the cell and the reference network density is 10 relays/km^2. The y-axis on the left, in blue, represents the densification gain and the y-axis on the right, in red, represents the aggregate rate gain. It can be observed that if the network density is doubled, PNC-B outperforms SC-PNC by about 22%. It can also be observed that as the network density increases, we get diminishing returns in terms of the aggregate rate gain. In addition, the rate gain for SC-PNC approaches that of the proposed PNC-B scheme only at very high relay densities. For instance, when the network density is increased 10-fold, the rate is doubled for both PNC-B and SC-PNC, when compared to the reference density of 10 relays/km^2.

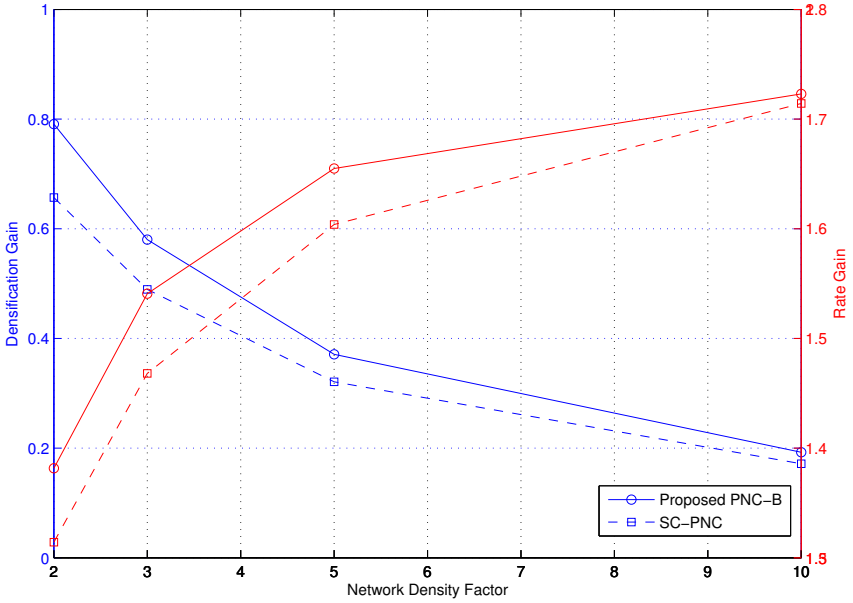

Fig. 5: Densification and Rate Gain Comparison

C. *Extension to the Multi-User Case*

When extending the relay selection algorithm to the multi-user case, there is a risk that the same relay may be selected for two or more users in the cell. This risk can be mitigated through proper scheduling. For illustration, let N_B be the maximum number of users that can be scheduled per transmission-time interval (TTI) and let N_{R_0} be the total number of relays deployed in the cell. The parameter N_B is determined by the number of resources available to the base station, such as the number of resource blocks as well as the number of transmitter and receiver antennas. The resources are then partitioned and allocated depending on the channel conditions perceived by each user. The problem of resource partitioning and allocation is however beyond the scope of this paper and is hence left for future work.

Without loss of generality, we assume that each relay is equipped with a single antenna. Multiple users could share the same relay if the relay is equipped with multiple antennas, as studied in [18]. Every scheduled user must have a unique relay assisting it. The number of users that can actually be scheduled per TTI, denoted as K, is then given by

$$K = \min\left(N_B, N_{R_0}\right) \tag{37}$$

Let $m_{i,j}$ be the generic scheduling metric for the i^{th} user in the j^{th} TTI. This metric is used to schedule the top K users during each TTI and is dependent on the scheduling algorithm.

For instance, if the maximum throughput algorithm is used, then $m_{i,j}$ will be the expected throughput of user i assuming that the optimum relay is selected at TTI j. This algorithm would then favour users that maximise the overall throughput of the system.

Given these parameters, Algorithm 2 extends Algorithm 1 to the single-cell, multi-user case. The first for-loop in the algorithm computes the scheduling metric for all the users in the cell. The scheduling metrics are then sorted in descending order and the top K users are scheduled. Once the users are scheduled, then the relays have to be selected in such a way that no two users share the same relay. This is handled by the second for-loop. The basic idea is that if there is a conflict where two users select the same relay, then the algorithm favours the user with the higher metric. The unfavoured user then selects a sub-optimum relay that is closest to the optimum. We have seen from Theorem 1 that this is the next best option.

In order to ensure fairness in the selection process, we use the proportional fair (PF) scheduling algorithm. In the PF algorithm, the scheduling metric is the expected throughput inversely weighted by the past average throughput [31]. This will ensure that users with good channel conditions and therefore higher expected throughput will not monopolise the relay selection process. Using PF, if a sub-optimum relay is selected for a user during one TTI, then it will be assigned a higher metric during the following TTIs until an optimum relay is selected for it.

We now compare the performance of our proposed algorithm with SC-PNC for the multi-user case. 30 users are uniformly distributed in the cell and Monte Carlo simulations of the algorithm are run over 1000 TTIs and 100 different network realisations. The average sum rate is then computed for the two approaches and it is plotted in Figure 6. The maximum number of users that can be scheduled per TTI (N_B) is assumed to be 15. Relays that are equidistant to each other are uniformly deployed in the cell. In addition, the time window over which fairness is imposed is set to 10 TTIs. The rest of the simulation setup is similar to that of the single-user performance study listed in Table I.

It can be seen from Figure 6 that the proposed PNC-B algorithm outperforms SC-PNC by about 21%. It can also be observed that the performance grows as the number of relays increases from 10 to 30. Beyond 30, we get diminishing returns when deploying more relays. When the number of relays N_{R_0} is 10, the number of users that are actually scheduled during each TTI is $K = \min(N_{R_0}, N_B) = 10$. This is less than the maximum number that can be scheduled per TTI and the performance is therefore limited by the relay deployment. As more relays are deployed, the performance improves and we see it plateauing when there are as

Algorithm 2: Relay Selection (Single-Cell, Multi-User)

Initialise metrics list $\mathbf{M}$ for all users in the cell with 0;
Initialise $\mathbf{O}_{R_0}$ with the optimum relays for all users in the cell using Algorithm 1;
Declare scheduled user list $\mathbf{S}_B$ of size K;
Declare scheduled relay list $\mathbf{S}_{R_0}$ of size K;
for *each user* i *in cell* **do**
    $\mathbf{M}[i]$ = Metric for user i at current TTI;
end
Sort list $\mathbf{M}$ in descending order;
$\mathbf{S}_B$ = Users corresponding to the top K metrics in sorted list $\mathbf{M}$;
for *each user* i *in* $\mathbf{S}_B$ **do**
    R_0^* = Optimum relay for user i from $\mathbf{O}_{R_0}$;
    if R_0^* *not in* $\mathbf{S}_{R_0}$ **then**
        $\mathbf{S}_{R_0}[i] = R_0^*$;
    else
        $\tilde{R}_0$ = Relay closest to R_0^* but not in $\mathbf{S}_{R_0}$;
        $\mathbf{S}_{R_0}[i] = \tilde{R}_0$;
    end
end
Return $\mathbf{S}_B$ and $\mathbf{S}_{R_0}$;

many relays as users. As a general rule of thumb, we recommend having a dense deployment of relays at areas in the cell with the maximum concentration of users. This is to ensure that the performance does not degrade too much even if a sub-optimum relay is selected. In the future, we will extend this study to the multi-antenna as well as the multi-cell cases.

V. PNC Decoding Performance with Power Imbalance

In the previous section, a relay selection algorithm for PNC-B that maximised the overall rate using the upper bound approximation was proposed. It was shown through simulations that it in turn maximised the achievable rate of the system assuming the use of nested lattice codes. A constraint on the transmitted powers was imposed where $P_A^{(t)} > P_{R_0}^{(t)} > P_B^{(t)}$, which is typical in a cellular network environment. This constraint may however lead to an

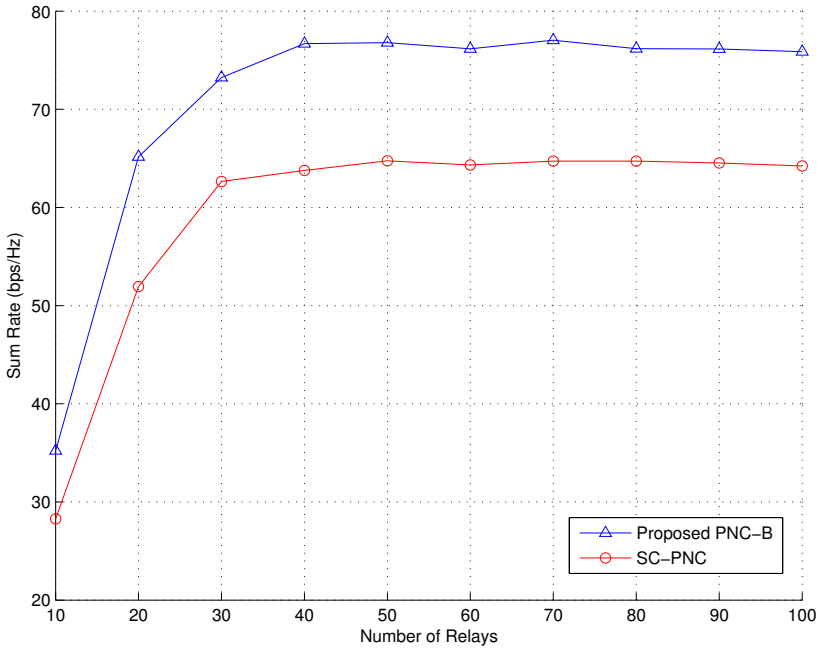

Fig. 6: Rate Performance Comparison for the Multi-User Case

imbalance in received SNRs at the relay in the multiple-access phase. In a PNC system, the multiple-access phase is key, since the network coded symbol received at the relay will determine the successful decoding of the individual transmitted symbols at the end nodes. This section studies the impact of this power imbalance on the decoding performance.

The decoding performance is defined as the rate at which the superimposed signal is successfully decoded by the relay in the multiple-access phase. We perform an experimental study of the decoding performance on the universal soft radio peripheral (USRP) platform in an indoor environment for the single-user case. The received power imbalance conditions of a cellular network are emulated, in this case by having the nodes transmit at different powers. This study serves to augment the theoretical work done in the previous section and to get us closer to implementing PNC in a practical cellular network.

A. Cumulative Distribution Function of the Received SNRs

Before describing the USRP experimental setup, a simulation-based study is done to obtain the cumulative distribution function (CDF) of the received SNRs at the relay for each of the links. The CDF will help us understand the likelihood of power imbalance at the relay in the multiple-access phase. It will also serve to guide the selection of the appropriate SNRs

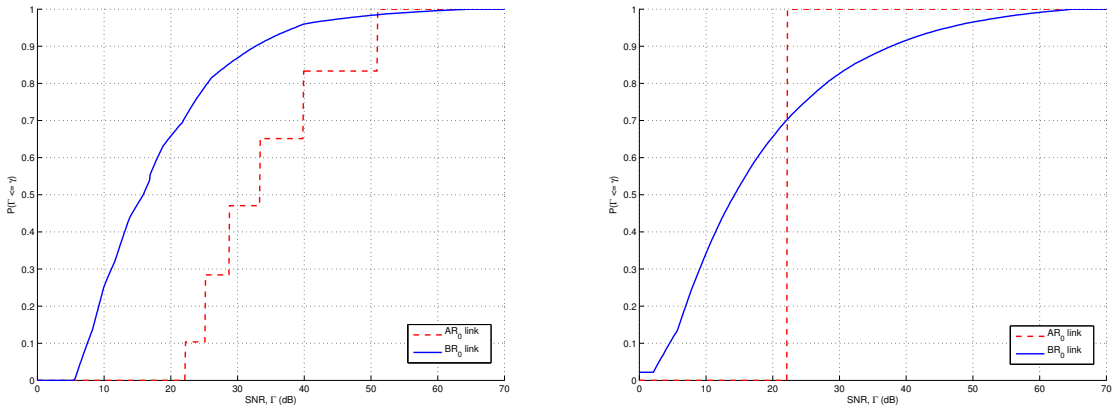

(a) Relay separation, s = 100m

(b) Relay separation, s = 600m

Fig. 7: CDF of SNRs Γ_{AR_0} and Γ_{BR_0} for PNC-B

for which experimental results will be collected from the USRP setup. The received SNR of the base station-relay link is denoted by Γ_{AR_0} and the received SNR of the user-relay link is denoted by Γ_{BR_0}. For the setup described in Section II, 100 users are uniformly distributed in the cell and the optimum relay for PNC-B is selected for each of the users. It is assumed that each user is scheduled at different time slots so that there are no conflicts in the optimum relay that is selected. The motivation of this study is to determine the received SNR at the relay for random user locations. Two different network deployments are considered: one in which the relays are densely deployed with a separation distance s = 100 m and the other in which s = 600 m. Rayleigh fading is considered and the received SNRs for 1000 different network realisations are obtained.

Figures 7a and 7b show the CDF of Γ_{AR_0} and Γ_{BR_0} for s = 100 m and s = 600 m respectively. The CDF of Γ_{BR_0} is a smooth curve since many users are considered and their locations are randomly distributed in the cell. The CDF of Γ_{AR_0} is piecewise linear. This is because the location of the base station is fixed and for a given user, there are only a certain number of relays to choose from in the cell. Since there are more relays to choose from in the dense deployment (s = 100m), Γ_{AR_0} has more steps. We define low, medium and high SNRs for a link xy to be the following:

1) Low SNR: $\Gamma_{xy} \leq 7.5$ dB
2) Medium SNR: 7.5 dB $< \Gamma_{xy} \leq 10$ dB
3) High SNR: 10 dB $< \Gamma_{xy} \leq 30$ dB

TABLE II: Probability of Low, Medium and High SNRs

CDF	Relay Separation	
	100 m	**600 m**
P(Γ_{AR_0} <= 7.5 dB)	0	0
P(Γ_{BR_0} <= 7.5 dB)	0.1	0.23
P(7.5 dB < Γ_{AR_0} <= 10 dB)	0	0
P(7.5 dB < Γ_{BR_0} <= 10 dB)	0.15	0.11
P(10 dB < Γ_{AR_0} <= 30 dB)	0.47	1
P(10 dB < Γ_{BR_0} <= 30 dB)	0.62	0.48

The probabilities for the low, medium and high SNRs for the AR_0 and BR_0 links are summarised in Table II. It can be seen that for the two network deployments, the probability that Γ_{AR_0} is low or medium is 0. This is because the base station is transmitting at very high power and in the worst-case the relay is only 600 metres away, which is within the boundary derived in Section IV-A. On the other hand, since the mobile is transmitting at low power, it is quite likely that Γ_{BR_0} is low (10% for s = 100m and 23% for s = 600m). As expected, the likelihood of a low Γ_{BR_0} is greater for a network with fewer relays.

B. Experimental Setup

We use the implementation of PNC on the USRP platform, detailed in [14], to analyse the decoding performance for various SNRs. The physical layer is based on OFDM and the cyclic prefix (CP) is used to resolve symbol asynchrony and prevent inter-symbol interference. The details of this and the frame format can be found in [14]. The modulation and coding schemes used by the end-nodes (A and B) are BPSK and convolutional coding as defined in the LTE standard [32, Chapter 10]. Since the decode-and-forward strategy is considered in this paper, link-by-link channel-coded PNC is implemented where the relay decodes the superimposed channel coded symbols from A and B and re-encodes it before broadcasting. Let the source symbols from nodes A and B be S_A and S_B respectively. After channel coding, the symbols X_A and X_B are transmitted in the multiple-access phase. The relay receives the superimposed coded symbols from A and B corrupted by noise. It then tries to decode $S_A \oplus S_B$ before re-encoding it for the broadcast phase. The XOR-Channel Decoder (XOR-CD) [14] is used at the relay. In XOR-CD, an XOR mapping of the received symbol Y to the transmitted network-coded symbol $X_A \oplus X_B$ is first performed, followed by channel decoding to obtain

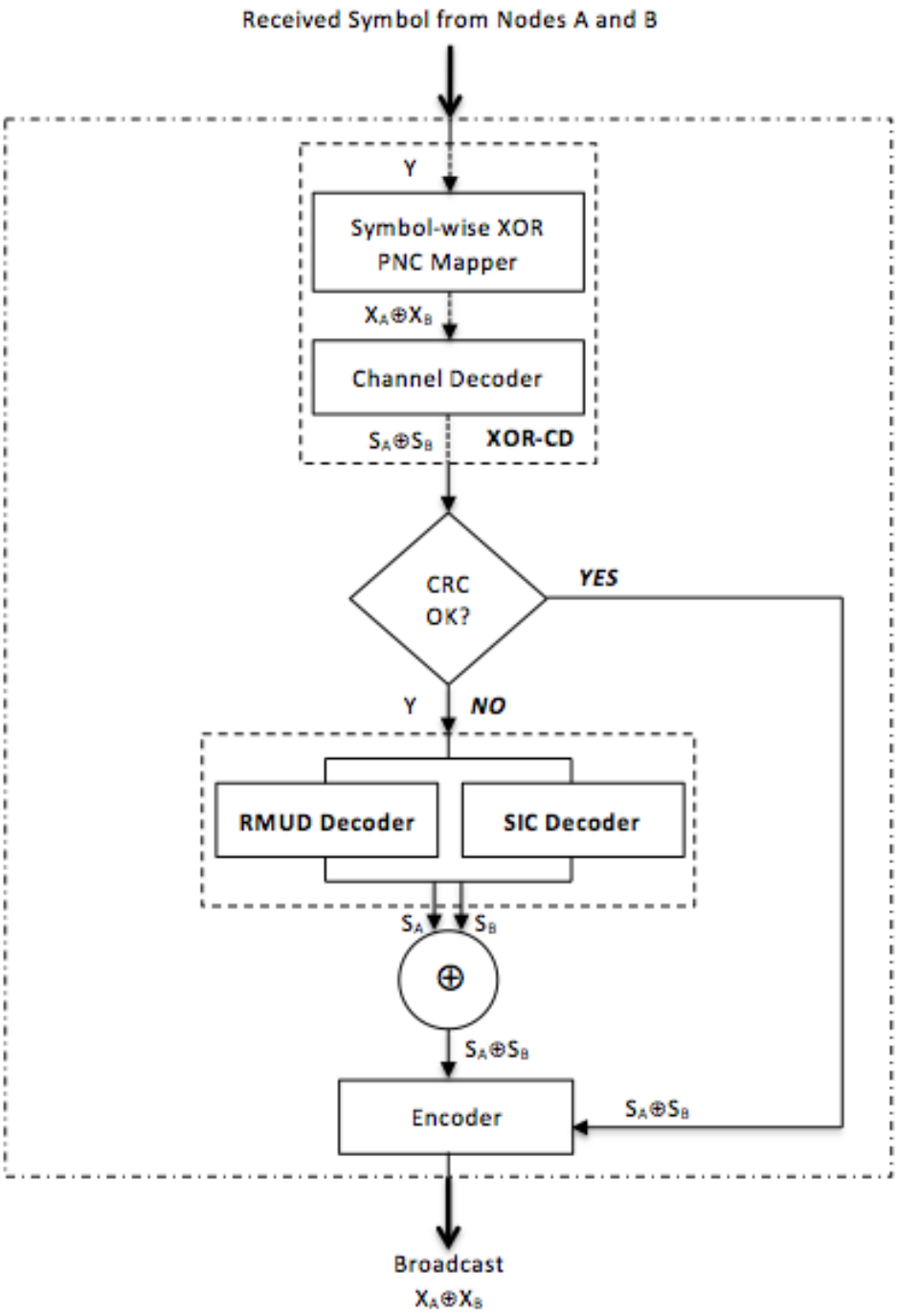

Fig. 8: Decoder Architecture at the Relay

$S_A \oplus S_B$. The channel decoder at the relay implements the Viterbi algorithm [14]. Error checking is also performed to verify if the decoding was successful. The IEEE CRC-32 (cyclic redundancy check) function is modified in the implementation so that CRC($S_A \oplus S_B$) = CRC(S_A) $\oplus$ CRC(S_B) [15].

If the channel decoding is unsuccessful (i.e. CRC check fails), two additional decoders are used to decode the individual source symbols S_A and S_B. The first decoder is based on reduced-constellation multi-user detection (RMUD) and the second is based on successful interference cancellation (SIC). In RMUD, the number of constellation points to consider for decoding is reduced by adopting the log-max approximation. In BPSK, for instance, the four possible constellation points $(\pm 1, \pm 1)$ are reduced to two, the details of which can be found in [33]. In SIC, the stronger signal is first decoded and the estimate of that is subtracted from the received signal to then decode the weaker one. If decoding is successful, both decoders would output S_A and S_B and they are then combined to form $S_A \oplus S_B$. Figure 8 gives an overview of the decoder architecture at the relay.

C. Decoding Performance

Figure 9 shows the decoding performance of XOR-CD alone and also the combined XOR-CD, RMUD and SIC decoders. The x-axis shows the received SNRs of the two end nodes at the relay. This is represented as an ordered tuple of the form $(\Gamma_{BR_0}, \Gamma_{AR_0})$ in dBs. It can be observed from the graph that at low SNRs, the decoding performance of XOR-CD is very low. It can also be observed that the decoding success rate improves when the received SNRs are imbalanced. For instance, for the (7,7.5) dB SNR pair, the success rate of XOR-CD is only about 10% and the success rate improves to about 33% for the (7,9) dB SNR pair. Similarly, the decoding performance of (7,9.5) dB is significantly greater than (7.5,7.5) dB. Since all the nodes are transmitting at maximum power, power control to balance the SNRs could be detrimental to the decoding performance, especially at low SNRs. At medium to high SNRs, the decoding performance of XOR-CD is between 88-95%. The success rate of XOR-CD could be further improved by using more advanced coding techniques.

The gain of using RMUD and SIC decoders over XOR-CD can be observed to be greater at low and medium SNRs and not so significant at high SNRs. This gain is quantified in Table III. We will look at the fourth row in the table to illustrate how the data can be analysed. For the SNR pair (7.5,9.5) dB, the gain provided by the RMUD and SIC decoders over XOR-CD is 6.9%. The contributions of RMUD and SIC toward this 6.9% gain are 10% and 97% respectively. The final column shows that both RMUD and SIC get 7% in common for successfully decoding the individual source symbols S_A and S_B.

We can now observe from Table III that at low and balanced SNRs, the success rate gain from RMUD and SIC is very low (between 0.1 and 1.2%). When the SNRs are imbalanced,

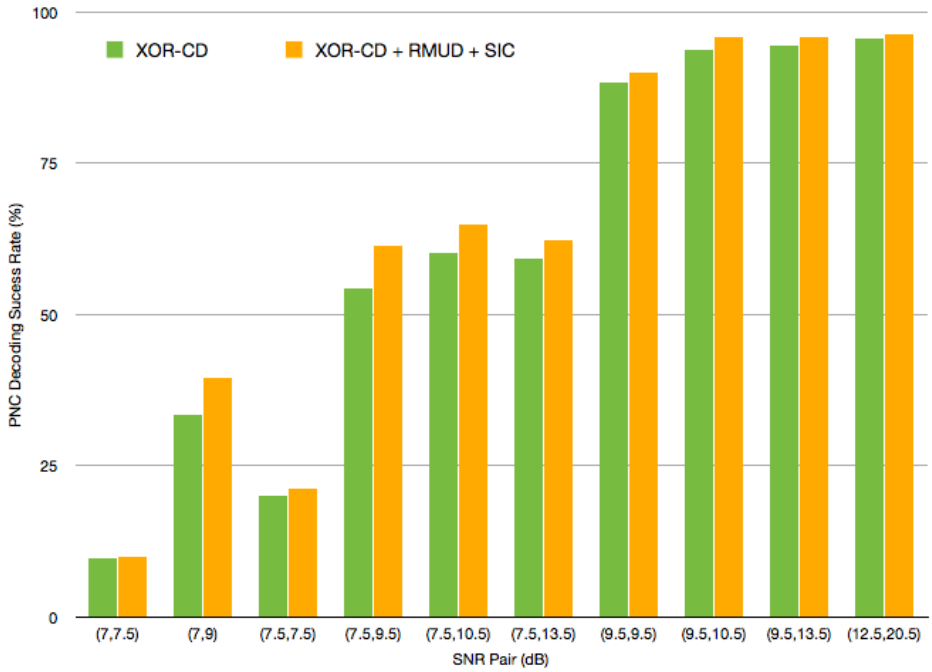

Fig. 9: PNC Decoding Performance at Relay

the contribution of RMUD and SIC is greater (between 4.6 and 6.9%), especially when the SNR from one of the nodes is low. It can also be observed that the contribution of SIC is significantly greater when there is an imbalance in SNRs. This is expected since SIC is designed to differentiate and decode the strong and weak signals.

TABLE III: Contribution of RMUD and SIC Decoders

SNR Pair (dB)	**Success Rate Gain from RMUD + SIC (%)**	**Contribution towards Gain**		
		RMUD (%)	**SIC (%)**	**RMUD ∩ SIC (%)**
(7,7.5)	0.1	100	0	0
(7,9)	6.1	0	100	0
(7.5,7.5)	1.2	25	75	0
(7.5,9.5)	6.9	10	97	7
(7.5,10.5)	4.6	9	96	5
(7.5,13.5)	3.1	15	87	2
(9.5,9.5)	1.7	30	90	20
(9.5,10.5)	2.2	47	76	23
(9.5,13.5)	1.5	27	91	18
(12.5,20.5)	0.8	27	86	13

These experimental results have practical implications and can be used by the network operator to make a tradeoff between cost and complexity. If cost in terms of relay deployment is an issue, then there will be fewer relays in the network resulting in the likelihood of a low Γ_{BR_0} to be higher. Then, the highly complex relay with XOR-CD+RMUD+SIC decoders have to be deployed to improve the decoding performance. If on the other hand complexity is an issue and the relay consists of XOR-CD only, then more relays have to be deployed to reduce the likelihood of a low Γ_{BR_0}.

VI. Conclusions and Future Work

This paper applies PNC in a heterogeneous cellular network with multiple relays to a single cell. For bidirectional traffic between the base station and the user, a relay-selection algorithm is proposed where uneven time allocations for the multiple-access phase and the broadcast phase are adopted to maximise the overall achievable data exchange rate. The optimisation problem is shown to be log-concave and relay selection is based on the gradient-ascent algorithm. Compared to the widely applied selection-cooperation technique, the proposed algorithm performs significantly better for all user locations and network deployments.

The decoding performance of PNC with imbalanced SNRs is then studied on the software radio platform. For the setup considered, the experimental results show that the decoding success rate improves when the received SNRs are imbalanced with channel coding. Since all the nodes are transmitting at maximum power, the results show that any power control to balance the SNRs could be detrimental to the decoding performance, especially at low SNRs. Two additional decoders based on multiuser detection and successive interference cancellation are also studied and when combined with the channel decoder, it is shown to improve the decoding performance at low and medium SNRs.

In the future, this study will be extended to a multi-cell setting with higher-order modulations and advanced coding techniques. The problem of resource allocation in the presence of fading will also be considered. The studies in this paper assumed an accurate estimate of the user location based on the received SNR. An accuracy study of these estimates based on real network data will be undertaken in the future as well.

Acknowledgement

The authors would like to acknowledge Toshiba Research Europe Ltd. (TREL) and the U.K. Research Council for supporting the work done in this paper through the Dorothy

Hodgkin Postgraduate Award. The authors would also like to thank the Worldwide Universities Network (WUN) Research Mobility Programme (RMP) for enabling the collaboration between the University of Bristol and The Chinese University of Hong Kong. This work is also partially supported by the General Research Funds (Project No. 414812) and AoE grant E-02/08, established under the University Grant Committee of the Hong Kong Special Administrative Region, China.

REFERENCES

[1] Cisco, "Visual Networking Index: Global Mobile Data Traffic Forecast Update," 2013. [Online]. Available: http://goo.gl/ZMbgJl

[2] I. F. Akyildiz, D. M. Gutierrez-Estevez, and E. C. Reyes, "The evolution to 4G cellular systems: LTE-Advanced," *Physical Communication*, vol. 3, no. 4, pp. 217–244, Dec. 2010.

[3] D. Gesbert, S. Hanly, H. Huang, S. Shamai Shitz, O. Simeone, and W. Yu, "Multi-cell MIMO cooperative networks: A new look at interference," *IEEE Journal on Selected Areas in Communications*, vol. 28, no. 9, pp. 1380–1408, 2010.

[4] E. Hossein, D. I. Kim, and V. K. E. Bhargava, *Cooperative Cellular Wireless Networks*. Cambridge University Press, 2011.

[5] Y. Peng and F. Qin, "Exploring Het-Net in LTE-Advanced System: Interference Mitigation and Performance Improvement in Macro-Pico Scenario," *IEEE ICC*, 2011.

[6] P. Bhat, S. Nagata, L. Campoy, I. Berberana, T. Derham, G. Liu, X. Shen, P. Zong, and J. Yang, "LTE-advanced: an operator perspective," *Communications Magazine, IEEE*, vol. 50, no. 2, pp. 104–114, 2012.

[7] S. Zhang, S. C. Liew, and P. P. Lam, "Hot topic: physical-layer network coding," *ACM Mobicom*, pp. 358–365, 2006.

[8] P. Popovski and H. Yomo, "The anti-packets can increase the achievable throughput of a wireless multi-hop network," in *IEEE ICC*, 2006, pp. 3885–3890.

[9] S. C. Liew, S. Zhang, and L. Lu, "Physical-layer network coding: Tutorial, survey, and beyond," *Physical Communication*, vol. 6, pp. 4–42, 2013.

[10] 3GPP, "Applications of network coding in LTE-A," *TSG-RAN 1 R1-090774*, 2009.

[11] ——, "Joint Analog Network Coding and Relay," *TSG RAN 1 R1-090065*, 2009.

[12] A. Osseiran, M. Xiao, S. B. Slimane, M. Skoglund, and J. Manssour, "Advances in wireless network coding for IMT-Advanced & beyond," *IEEE International Conference on Wireless VITAE*, 2011.

[13] L. Lu and S. C. Liew, "Asynchronous physical-layer network coding," *IEEE Transactions on Wireless Communications*, vol. 11, no. 2, pp. 819–831, 2012.

[14] L. Lu, T. Wang, S. C. Liew, and S. Zhang, "Implementation of physical-layer network coding," *Physical Communication*, vol. 6, pp. 74 – 87, 2013.

[15] L. Lu, L. You, Q. Yang, T. Wang, M. Zhang, S. Zhang, and S. C. Liew, "Real-time implementation of physical-layer network coding," *Proceedings of the second workshop on Software radio implementation forum*, pp. 71–76, 2013.

[16] M. Wu, M. Woltering, D. Wuebben, A. Dekorsy, F. Ludwig, and S. Paul, "Analysis and Implementation for Physical-Layer Network Coding with Carrier Frequency Offset," in *International ITG Workshop on Smart Antennas*, 2014, pp. 1–8.

[17] S. Zhang, C. Nie, L. Lu, S. Zhang, and G. Qian, "MIMO Physical Layer Network Coding Based on VBLAST Detection," *International Conference on WCSP*, pp. 1–5, 2012.

[18] Z. Ding, I. Krikidis, J. Thompson, and K. K. Leung, "Physical layer network coding and precoding for the two-way relay channel in cellular systems," *IEEE Transactions on Signal Processing*, vol. 59, no. 2, pp. 696–712, 2011.

[19] R. H. Y. Louie, Y. Li, and B. Vucetic, "Practical Physical Layer Network Coding for Two-Way Relay Channels: Performance Analysis and Comparison," *IEEE Transactions on Wireless Communications*, vol. 9, no. 2, pp. 764 – 777, 2010.

[20] L. Song, G. Hong, B. Jiao, and M. Debbah, "Joint Relay Selection and Analog Network Coding Using Differential Modulation in Two-Way Relay Channels," *IEEE Transactions on Vehicular Technology*, vol. 59, no. 6, pp. 2932 – 2939, 2010.

[21] S. Katti, S. Gollakota, and D. Katabi, "Embracing Wireless Interference: Analog Network Coding," *SIGCOMM*, 2007.

[22] M. Ju and I.-M. Kim, "Relay Selection with Physical-Layer Network Coding," in *IEEE Globecom*, 2010, pp. 1–5.

[23] A. Bletsas, H. Shin, and M. Z. Win, "Cooperative communications with outage-optimal opportunistic relaying," *IEEE Transactions on Wireless Communications*, vol. 6, pp. 3450–3460, 2007.

[24] E. Beres and R. Adve, "Selection cooperation in multi-source cooperative networks," *IEEE Transactions on Wireless Communications*, vol. 7, pp. 118–127, 2008.

[25] W. Nam, S.-Y. Chung, and Y. H. Lee, "Capacity of the Gaussian two-way relay channel to within 1/2 bit," *IEEE Transactions on Information Theory*, vol. 56, no. 11, pp. 5488–5494, 2010.

[26] H. Xu and B. Li, "An Optimization Framework for XOR-Assisted Cooperative Relaying in Cellular Networks," *IEEE Transactions on Mobile Computing*, pp. 1– 14, 2013.

[27] S. P. Boyd and L. Vandenberghe, *Convex Optimization*. Cambridge University Press, 2004.

[28] 3GPP, "Evolved Universal Terrestrial Radio Access (E-UTRA): Further advancements for E-UTRA physical layer aspects," *TR 36.814 v9.0.0*, 2010.

[29] ——, "Radio Measurement Collection for Minimization of Drive Tests (MDT) (Release 11)," *TS 37.320 v11.1.0*, 2012.

[30] J. Andrews, S. Buzzi, W. Choi, S. Hanly, A. Lozano, A. Soong, and J. Zhang, "What will 5G be?" *IEEE Journal on Selected Areas in Communications*, vol. 32, no. 6, pp. 1065 – 1082, 2014.

[31] F. Capozzi, G. Piro, L. Grieco, G. Boggia, and P. Camarda, "Downlink packet scheduling in LTE cellular networks: Key design issues and a survey," *IEEE Communications Surveys & Tutorials*, vol. 15, no. 2, pp. 678–700, 2013.

[32] S. Sesia, I. Toufik, and M. Baker, *LTE: The UMTS Long Term Evolution*. New York: John Wiley & Sons, 2009.

[33] L. Lu, L. You, and S. C. Liew, "Network-Coded Multiple Access," *IEEE Transactions on Mobile Computing*, vol. 13, no. 12, pp. 2853–2869, 2014.